

We are IntechOpen, the world's leading publisher of Open Access books Built by scientists, for scientists

5,500

Open access books available

136,000

International authors and editors

170M

Downloads

Our authors are among the

154

Countries delivered to

TOP 1%

most cited scientists

12.2%

Contributors from top 500 universities



WEB OF SCIENCE™

Selection of our books indexed in the Book Citation Index
in Web of Science™ Core Collection (BKCI)

Interested in publishing with us?
Contact book.department@intechopen.com

Numbers displayed above are based on latest data collected.
For more information visit www.intechopen.com



Effect of Piezoelectric Field on the Optical Properties of (311) A and (311) B Oriented InAlAs/InP Heterostructures

Badreddine Smiri, Faouzi Saidi and Hassen Maaref

Abstract

InAlAs alloy was grown by MOCVD on an InP (311) substrate with different polarities. Measurements of photoluminescence (PL) and photoreflectance (PR) were performed to study the impact of the V/III flux ratio. It is discovered that the PL line was shifted to a greater energy side with the increasing excitation power density, and no saturation was observed of its related PL intensity. It is a fingerprint of type II transition emission. However, the recombination of the type II interface showed a powerful dependence on AsH₃ overpressure and substrate polarity. In fact, we have noted an opposite behavior of type II energy transition shift from A to B polarity substrate in respect to V/III ratio variation. PR signals corresponding to Franz-Keldysh Oscillation (FKO) were observed. The analysis of their period has allowed one to assess the value of the PZ field in the samples. PL-luminescence measurements were performed out as a function of temperature. PL peak energy, PL intensity, and half maximum full width show anomalous behaviors. Indicating the existence of localized carriers, they were ascribed to the energy potential modulation associated with the indium cluster formation and PZ field.

Keywords: V/III flux ratio, substrate polarity, piezoelectric field, Franz-Keldysh oscillation, photoreflectance, photoluminescence

1. Introduction

Recently, scientists have focused their interest in InAlAs/InP grown on non-conventional (n11) planes. For example, (311) A and (311) B are not acquired as compared to the used (001) surface due to their remarkable characteristics [1]. In addition, InAlAs semiconductor layers grown on (311) A/B-oriented InP substrates give several unique characteristics compared to those grown on InP (100). Indeed, in (311) plane, the strain and hydrostatic deformations are discovered to be improved compared to those on (100) plane [1–3]. The primary reasons for this are: (i) the presence of a built-in electric field, produced through the piezoelectric effect in the layer [1, 4, 5] and (ii) the difference in arsenic segregation at the inverse interface. It is expected that these factors will be heavily dependent on growth conditions such as substrate orientation, V/III ratio.

InAlAs-InP materials have attracted tremendous interest over the past decades due to a variety of potential applications such as optical, optoelectronic and

electronic devices [6, 7] due to its large direct band-gap energy, high electron mobility and the type II nature of the interface [8]. These advancement efforts were appointed by the fabrication and commercialization of a variety of devices such as Quantum cascade lasers (QCLs) [9, 10], Avalanche Photodiodes (APDs) [11] and high-electron-mobility transistor (HEMT) [12–14]. The heterostructures of $\text{In}_x\text{Al}_{1-x}\text{As}/\text{InP}$ have a type II transition [1, 15] which becomes a promising contender for the optical telecommunication light source. Different techniques such as Molecular Beam Epitaxy (MBE) and Metal-Organic Chemical Deposition (MOCVD) have developed this type of structure. However, the InAlAs material itself suffered from a large density of hetero-epitaxy-inherent defects [1, 6]: (i) Al content, (ii) phase separation, and (iii) InAlAs growth spinodal decomposition. Despite all this, the full potential of devices based on InAlAs/InP has still been obtained.

These issues are expected to be highly dependent on growth conditions (substrate polarity, V/III ratio, etc.) due to the large difference in bond energy between Al-As and In-As [15]. To date, most study work on the optical and electrical properties of InAlAs was performed on the conventional (100) planes, but little is known for the non-conventional (n11) planes. Different substrate orientations show various surface states, which are expected to influence the growth mode and even the optical and electrical properties of epilayers.

The existence of aluminum in the InAlAs layer, therefore, prompts the existence of the In- and Al-rich clusters, which is the consequence of the non-uniformity in the alloy composition. As a result, it contributes to the undulation of the InAlAs bandgap from which the localized energy level is present. In addition, the substrate polarity [A or B] in our nanostructures alters the containment of electrons-holes by changing the strain and the existence of piezoelectric (PZ) field within the structure. Similar heterostructures such as $\text{In}_{0.21}\text{Ga}_{0.79}\text{As}/\text{GaAs}$ (311) A MQWs [16] and heterostructures AlGaAs/GaAs grown on (100), (311) A and (311) B-oriented substrates [17] have seen the carrier localization phenomenon. The previous investigation will be constrained to those samples implanted at high index (11N). We have shown in our latest study [18] that the presence of localized carriers has been attributed to the energy potential modulation related to the existence of Indium clusters and PZ-field.

The aim of our chapter is to study the effect of PZ-field on the optical properties of InAlAs/InP (311) with different substrate polarity, elaborated by MOCVD. The research of their optical characteristics by PR and PL spectroscopy is a significant step to demonstrate the possibility of incorporating our structure into optoelectronic applications such as 1.55 μm devices.

2. Experimental details

The studies are conducted on InP/InAlAs/InP (311) double heterostructures, marked as S1, S1', S1'', S2, S2' and S2'', which are cultivated at different V/III ratios by low-pressure metal-organic chemical vapor deposition (MOCVD). More information about development is summarized in **Table 1**. The source materials for the growth process are trimethylindium (TMIn), trimethylaluminum (TMAI) and (AsH₃). At a substrate temperature of 600°C, an InP layer of 100 nm thickness was developed. The growth rate of InP is approximately 0.17 nm/s. A 270 nm thick layer of $\text{In}_x\text{Al}_{1-x}\text{As}$ was subsequently deposited. Each sample was finally capped with an InP layer of 10 nm.

The source of excitation is the 514.5 nm line of the continuous-wave Ar⁺ laser with an excitation density of 80 W/cm² in PL measurements. Spectral analysis of

Samples	Substrate orientation	V/III ratio molar
S1	(311) B	25
S1'	(311) B	50
S1''	(311) B	125
S2	(311) A	25
S2'	(311) A	50
S2''	(311) B	125

Table 1.
 Growth conditions of the samples S1, S1', S1'', S2, S2' and S2''.

the luminescence measurements was performed out using JOBIN YVON HRD1 monochromatic and identified by a cooled Ge diode detector with a built-in amplifier. PR measurements were performed using a standard setup with the 514.5 nm line of Ar⁺ laser as the pump light, which was mechanically chopped at 970 Hz. The probe light was acquired from a 250 W tungsten halogen lamp dispersed with a 275 mm focal length monochromatic. The reflectance signal is detected by an InGaAs and silicon photodiodes.

3. Results and discussions

3.1 Photoluminescence study

3.1.1 Effect of substrate polarity: PZ-field

PL spectra were registered at low temperature to confirm the effect of PZ-field on the optical properties of InAlAs/InP (311) A/B:

Figure 1 illustrates the 10K-PL spectra of InAlAs/InP samples grown on (311) B and (311) A, respectively denoted S1 and S2. A higher energy side, both emissions at around 1.13 and 1.23 eV, for the samples S1 and S2, can be related to the interfacial defects between the InAlAs and InP layers [1, 19]. Both PL bands occur at about 0.8 and 1.03 eV for S1 and S2, respectively, on the lower energy side. A gradual InAs_xP_{1-x} layer formation at the interface between InP and InAlAs (see **Figure 2**) was explained by Hallara et al. [6]. For sample S1, an emission situated at around 1.27 eV may be related to acceptor-band recombination [1].

To analyze the origin of the inverted interface (InP/InAlAs), we suggested a model based on arsenic segregation (some atomic monolayers) and linked the theoretical calculations with the experimental results.

We can conclude that the radiative recombination around the inverse interface with emission 1.03 eV for the polarity A is due to the appearance of a gradual layer for 3ML of InAs_xP_{1-x}. In this case, the arsenic content of xAs is about 40%, but in the inverted transition for polarity B, it is in the order of 70%. It is possible to estimate the band offset between InP and In_{0.513}Al_{0.487}As layers based on this reference [20]. In fact, the interface between InP and InAs_xP_{1-x} layers is type I, although it is type II for In_{0.513}Al_{0.487}As and InAs_xP_{1-x}, where the xAs content ranged from 0 to 0.78.

There are two Gaussian peaks in the PL spectrum (see **Figure 1**). For the type II transition, an asymmetric band tail appeared in both S1 and S2 samples, resulting from unintentional thin strained InAs layers created at the InAlAs-InP interface [1, 18]. To explain more, this layer's smaller band gap can conduct a quantum well

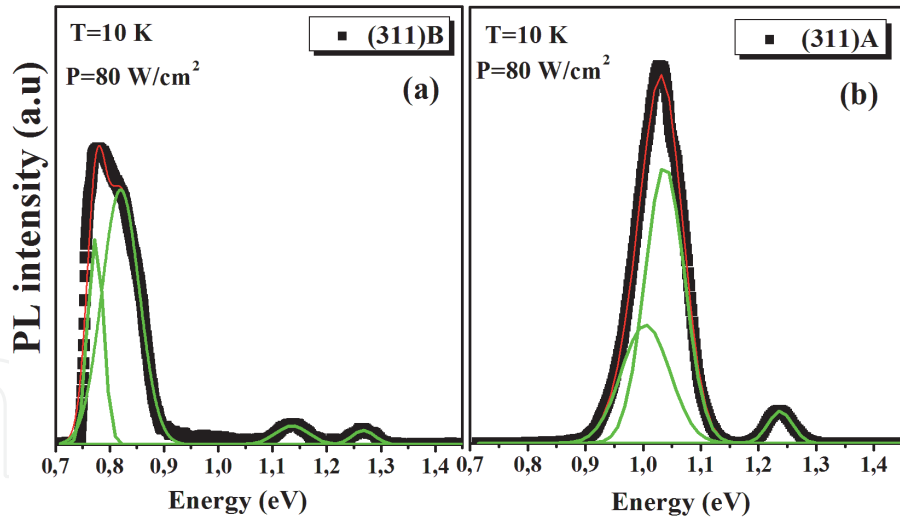


Figure 1. (a) and (b) Low temperature PL spectra of InAlAs on InP (311) A and on InP (311) B, respectively. The green solid line is the Gaussian-fitting curve.

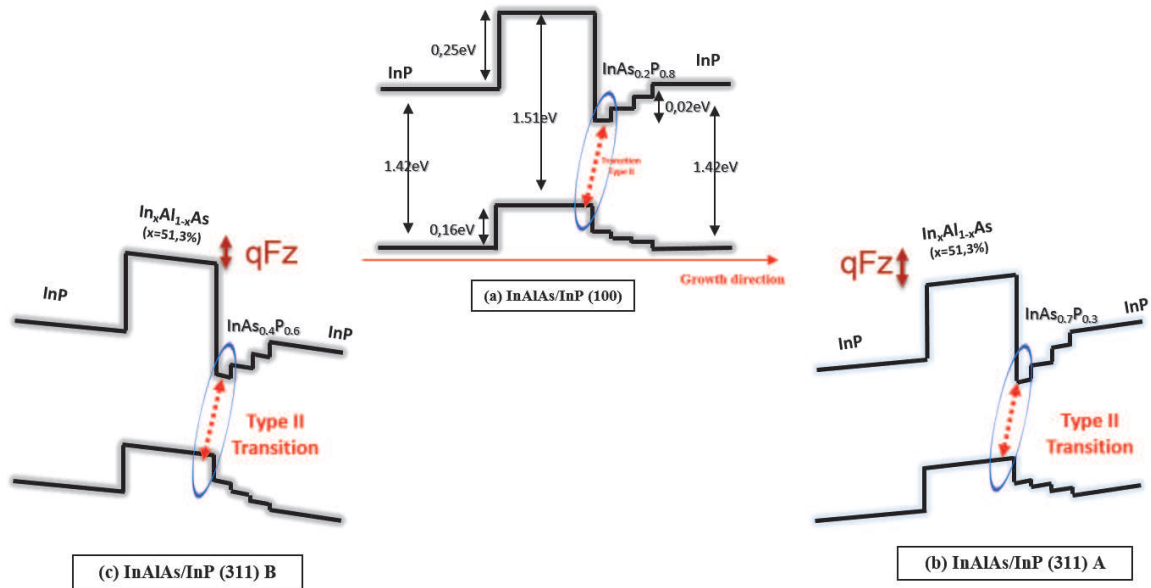


Figure 2. (a) Schematic band diagrams for sample of InAlAs on InP (100), (b) on InP (311) A, and (c) on InP (311) B.

at the interface, resulting in a mixed type I–II transition [21]. We notice that the difference in energy between the two transitions type II corresponds to the difference in arsenic atoms surface segregation. Thus, depending on the growth axis, this energy shift can be attributed to the piezoelectric field [1, 5]. In addition, the existence of defect states may function as non-radiative centers resulting in a decrease in PL intensity. We should note that as mentioned at the beginning of this chapter, these defects originated from the development process as well as doping. Added to this, the sample cultivated on the (311) B surface has a greater residual impurity concentration than the samples cultivated on the (311) A surface [17]. For the (311) A sample, therefore, the interface quality is considered better than that for the (311) B sample.

3.1.2 Effect of V/III flux ratio

To verify the impact of V/III ratio on the optical properties of InAlAs/InP (311) A/B, PL spectra were recorded at low temperature.

Figure 3 shows PL spectra at 10 K of the studied samples on different oriented InP substrate and at various V/III molar ratio. PL spectra are normalized and deconvoluted into various Gaussian curves for the convenience of comparison and to

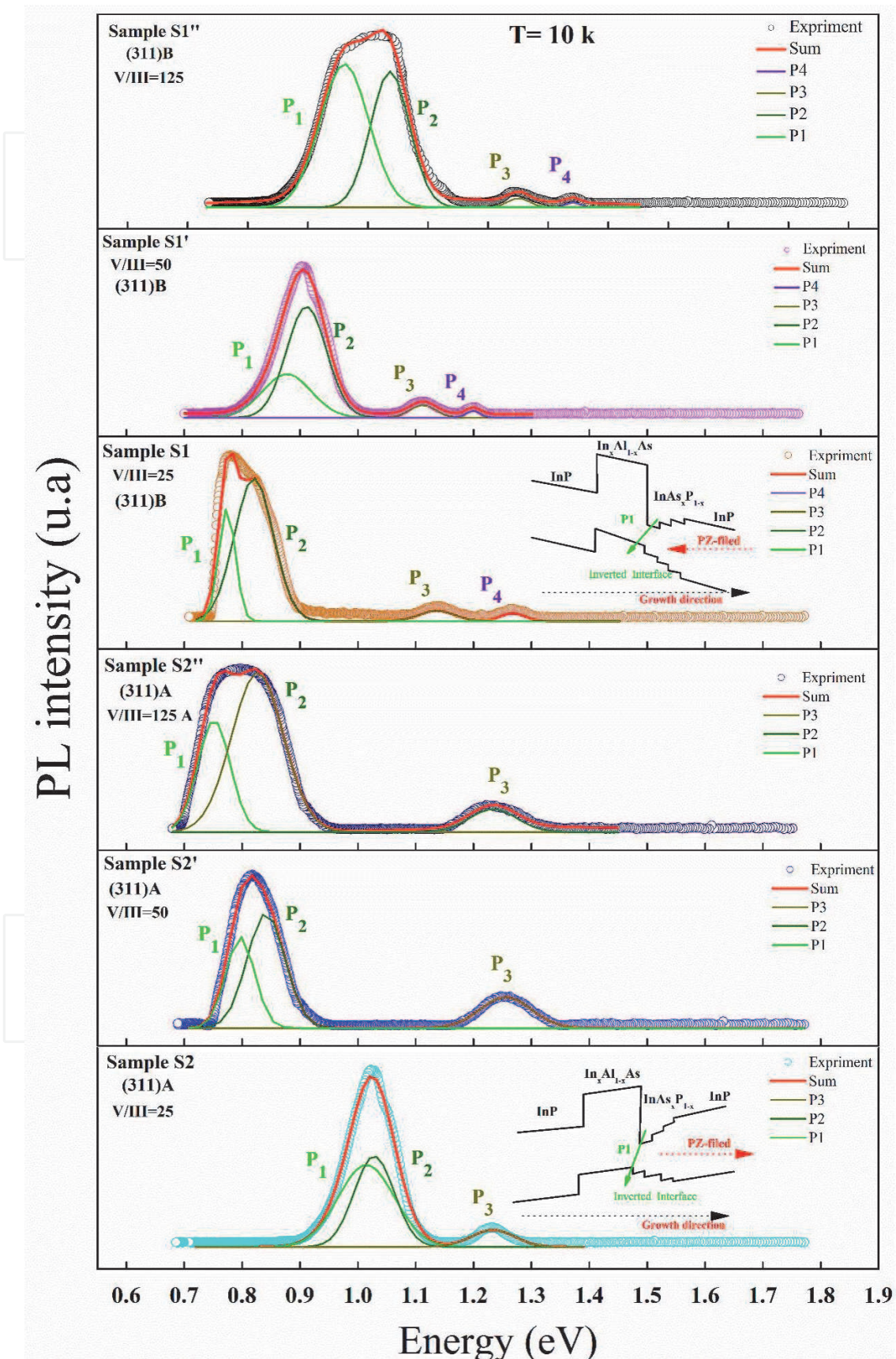


Figure 3. Low-temperature (10 K) PL for samples S1, S1', S1'', S2, S2' and S2''. In order to identify the different emission peaks, the spectra are normalized and deconvoluted by a multiple Gaussian curve fitting. Inset shows the schematic band diagram showing the radiative transitions from the type II transition (P1).

identify the different emission peaks. The spectra show four significant emission peaks marked as P1, P2, P3 and P4 for the (311) B sample. The P1 position is attributed to the type II emission across the interface between the two-dimensional electron states in thin $\text{InAs}_x\text{P}_{1-x}$ graded layer at the inverted interface and holes located on top of the InAlAs valence band [1]. The intermediate layer of InAsP consists of the higher coefficient of incorporation of As compared to P [1, 5, 18]. Numerous investigations have shown that the type II emissions in InAlAs-InP heterostructures observed in the 0.8–1.25 eV range [1, 20, 22]. This very broad variety conceals some general patterns that appear to be related to conditions of growth. Whereas, the peak P2 emission is associated with a mixed type I–II transition and else P3 peak can be related to the interfacial defects in InAlAs/InP emission [1]. Finally, the P4 peak situated in the PL spectrum at a greater energy side for (311) B samples can be ascribed to acceptor-band recombination [5]. See our first part above for more information.

On the other hand, for (311) A plane, the peak P4 of all samples is not observed in PL spectra, which may be attributed to the existence of composition modulation in the epitaxial layer of InAlAs with varying molar ratio and substrate polarity. Sayari et al. [23] performed a Raman research study of the impact of the V/III flux ratio in heterostructures of InP/InAlAs/InP. The research demonstrates that the quantity of clustering is envisaged to depend on conditions of development such as substrate polarity, V/III ratio, etc.

Figure 4 exhibits the variation in the type II transition energy as a function of the V/III molar ratio for samples cultivated on (311) A and (311) B. For the (311) orientation, the peak position depends upon whether the substrate is In terminated (A-face) or P terminated (B-face). The variation of type II transition energy (P1) was acting differently with the V/III ratio, according to the substrate polarity. For the B-face (samples S1, S1' and S1''), the P1 emission peak energy tends to increase as the V/III ratio decreases [5]. Whereas for the A-face (samples S2, S2' and S2''), we noted a decrease in the P1 emission peak as the V/III ratio increases (i.e. a blue shift is observed for (311) B samples [5], while red shift is noted for (311) A samples). These findings could possibly be clarified by the meaning of a piezoelectric field in InAlAs/InP heterostructures resulting from the difference between the atomic terminated surface [A or B] in InP substrate differences in interface reconstructions [1]. The PL shift can simply be attributed to the type of atoms present on the surface,

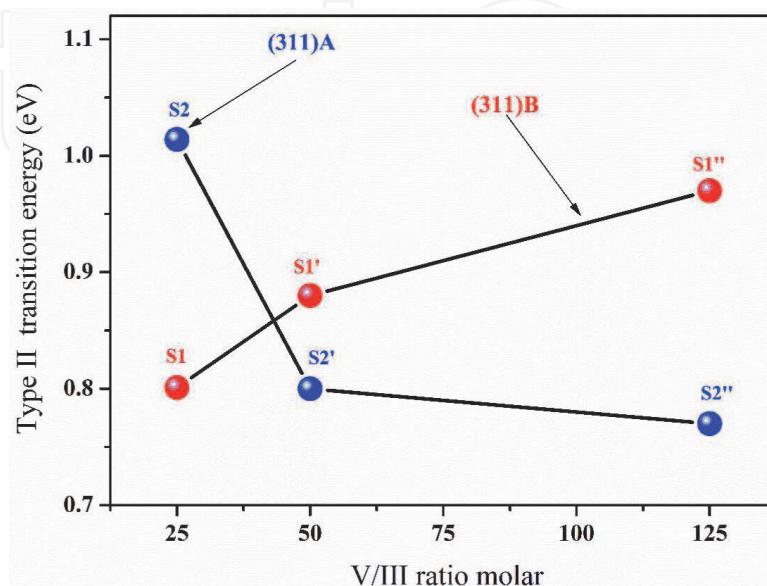


Figure 4. Variation of the type-II transition energy as a function of V/III ratio for the (311) A and (311) B substrate orientation.

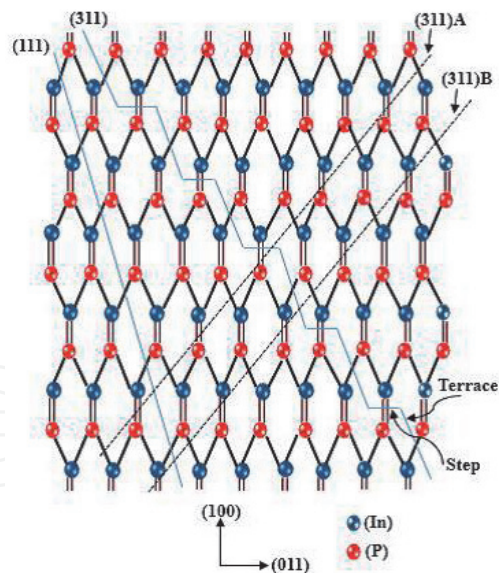


Figure 5.
 Illustration of (311) A and (311) B planes of InP.

resulting in different levels of confinement. There are two types of sites on the surface (311): one is the double bond site found in the direction [100] and the other is a single bond site found in the direction [111], their densities being precisely the same [5]. On a (311) A surface, the double dangling bond sites are In sites and the single dangling bond sites are P sites, but on a (311) B surface the double dangling bond sites are P sites and the single dangling bond sites are In sites (see **Figure 5**) [19, 24, 25]. These completely distinct configurations of plane bonding are eventually responsible for the meaning of the PZ field on the different planes. Furthermore, the study of the impacts of InP substrate polarity shows that As incorporation (arsenic diffusion) may be improved on (311) A samples but may be decreased on (311) B samples with an increased V/III ratio. It can be shown from Ref. [20] that the increase in arsenic composition (InAsP) will reduce the transition energy of type II.

3.1.3 Power-dependent photoluminescence (PDPL)

We studied the evolution of the PL peak energy as PDPL, as shown in **Figure 6**, to verify these assignments. The energy blue changes with increased excitation

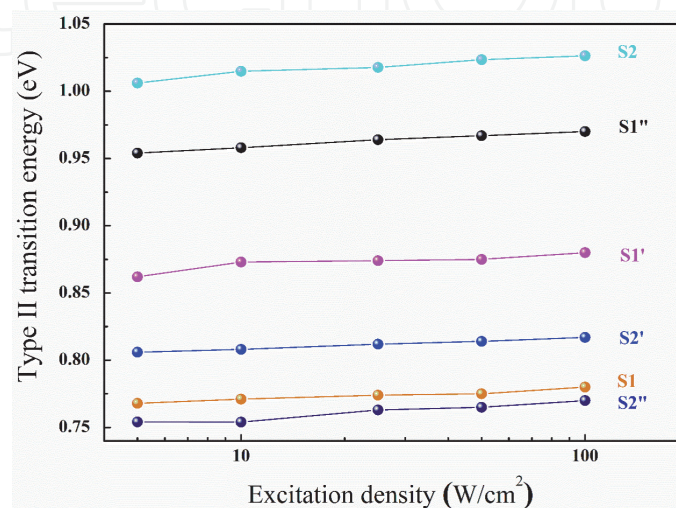


Figure 6.
 The PL emission energy for the type II transition of all samples as a function of excitation power densities.

power intensity for type transition. This conduct is associated with recombination of type II via an interface with other material structures such as GaAsSb/InP [26, 27] and GaSb/InGaAs [28].

The following Eq. (1) was used to estimate the nature of the recombination around the InP/InAlAs inverse interface [1]:

$$I_{PL} = (P_{exc})^n \quad (1)$$

where P_{exc} is the power excitation, IPL is the integrated PL intensity and n is an exponent.

We found that the exponent n close to the unity. At higher power of excitation, there is no saturation. This shows that this PL transition is not attributable to impurity or defects, but is intrinsic recombination (band-to-band) [1]. **Figure 6** indicates a logarithmic linear dependence of the PL peak energy of the inverse interface with the density of excitation power. Hallara et al. [6] noted this behavior. Additionally, **Figure 6** display that the blue-shifted with the increase of the excitation power density. The offset is approximately 7 meV. This shows that the change of emission energy with increasing excitation power is also proof to verify our hypothesis (carrier localization) and PZ-filed presence in our structures [18].

A final analysis based on the PL temperature was created to further verify our hypothesis. In both samples, we can gain greater insight into the carrier localization and the mechanism of luminescence.

3.1.4 Temperature-dependent photoluminescence (TDPL)

Scientific study shows that two factors are noted for conventional orientation (100), at low temperature 10 K and with aspect ratio V/III equivalent to 50, two factors are observed: (i) clusters formation and (ii) composition modulation leading to natural superlattice [6]. Some scientists discovered that the latter factor disappears and if the ratio V/III changes [5, 6, 22], the clustering impact remains only.

It related to the phenomenon of exciton location. Carefully research as a function of PL temperature is conducted to demonstrate our hypothesis.

In both samples (S1 and S2) mentioned above, the PL peak energy-temperature reliance obtained from PL spectra is shown in **Figure 7(a)** and **(b)**. The PL spectrum (inset **Figure 7**) is revealed between 10 and 300 K. The so-called S-shaped temperature dependence of emission energy is obviously shown as a successive reform to low-high-low energy. It displays anomalous behavior as a temperature function. This behavior is characteristic of localization effects, and has been already observed in InAlAs alloys on InP [29, 30], GaAsSb/InP layers [31], BGaAs/GaAs layers [32, 33] and In_{0.21}Ga_{0.79}As MQWs on GaAs (311) A [16].

The S-shaped shape in PL peak energy can be separated into three primary intervals of temperature and is interpreted as follows: at the low-temperature range, the excitons should be situated in the levels whose distribution goes into the material's prohibited band. This is called band tails, associated with cluster appearance in the InAlAs [18]. With growing temperature, the excitons get enough thermal energy to reach deeper localized states and recombine primarily from low energy levels, resulting in a dramatic red shift (part I). Indeed, when the temperature increases, the thermal energy becomes adequate for the excitons in the tails to attain the corners of the stripes, where they are delocalized to high levels of energy. A blue shift is noted as a consequence (part II). All carriers are delocalized to the continuum at the high-temperature region, where band-band transitions are favored (part III) [18].

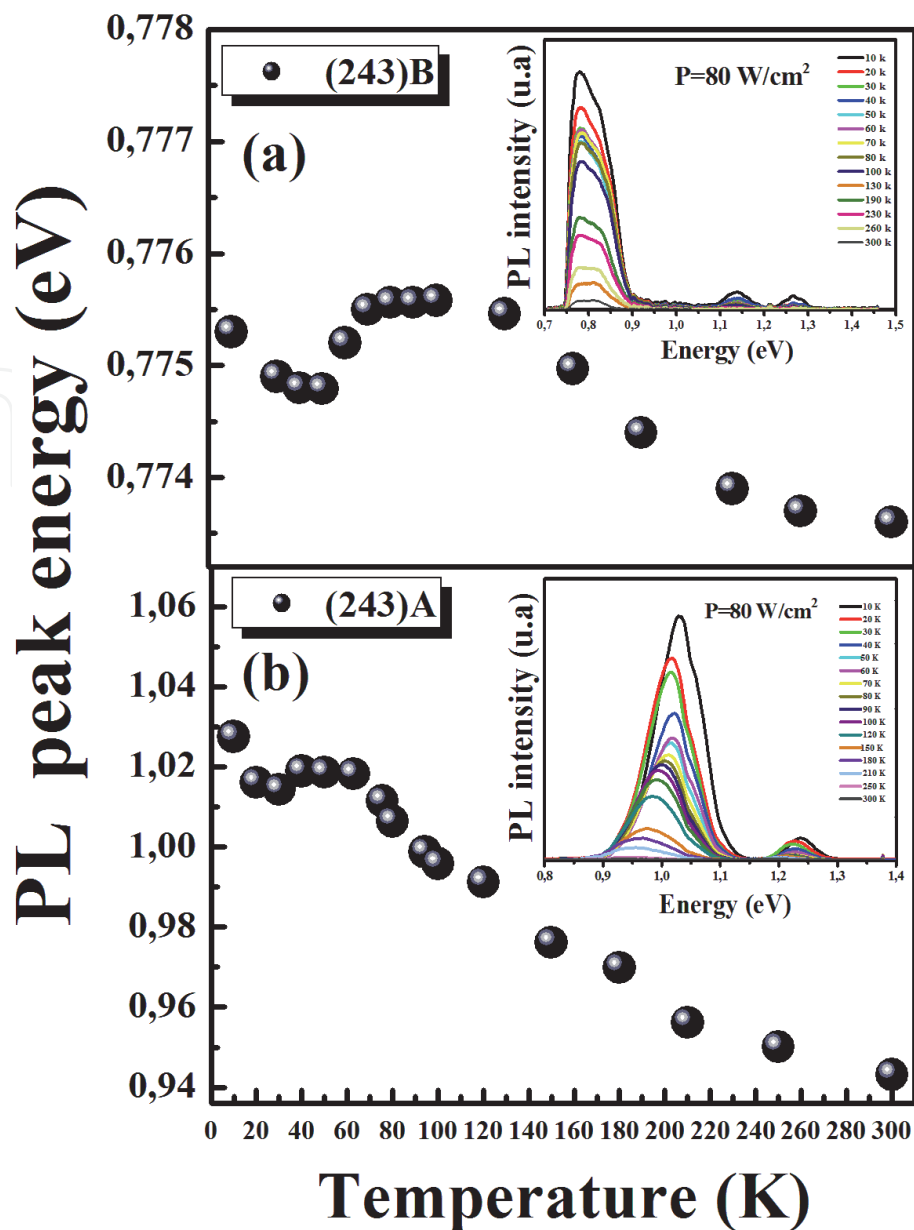


Figure 7.
 (a) and (b) experiment data for the temperature dependence of Transition type II emission in $\text{In}_{0.513}\text{Al}_{0.487}\text{As}$ grown on InP (311) B and on InP (311) A substrates, respectively.

Another main parameter of the presence of the localization phenomenon is the Full width at Half Maximum (FWHM) behavior. Indeed, compared to the classic III-V semiconductor alloys, it demonstrates atypical behavior. It shows an inverted “N-shape” (decrease-increase-decrease) (see **Figure 8**). The excitons are localized in the potential minima at cryogenic temperature. The carriers gain more thermal energy at intermediate temperatures to overcome the tiny energy barriers and attain greater energy states. As the temperature increases further, the FWHM broadening is described as the interaction of the electron-phonon. Finally, up to room temperature, the line width decreases continuously. It demonstrates the inverse trend of expanding optical phonons [1, 18]. This behavior can be clarified by the thermo-activation of the carriers and their transfer between nearby fluctuation potentials induced by the inhomogeneous distribution. Indeed, the carriers that are being thermally activated into a small potential can be further retrapped by the large one [18].

As a function of temperature, the S-shape in PL peak energy is not clear in polarity B as polarity A. The reason for this distinction can be clarified by

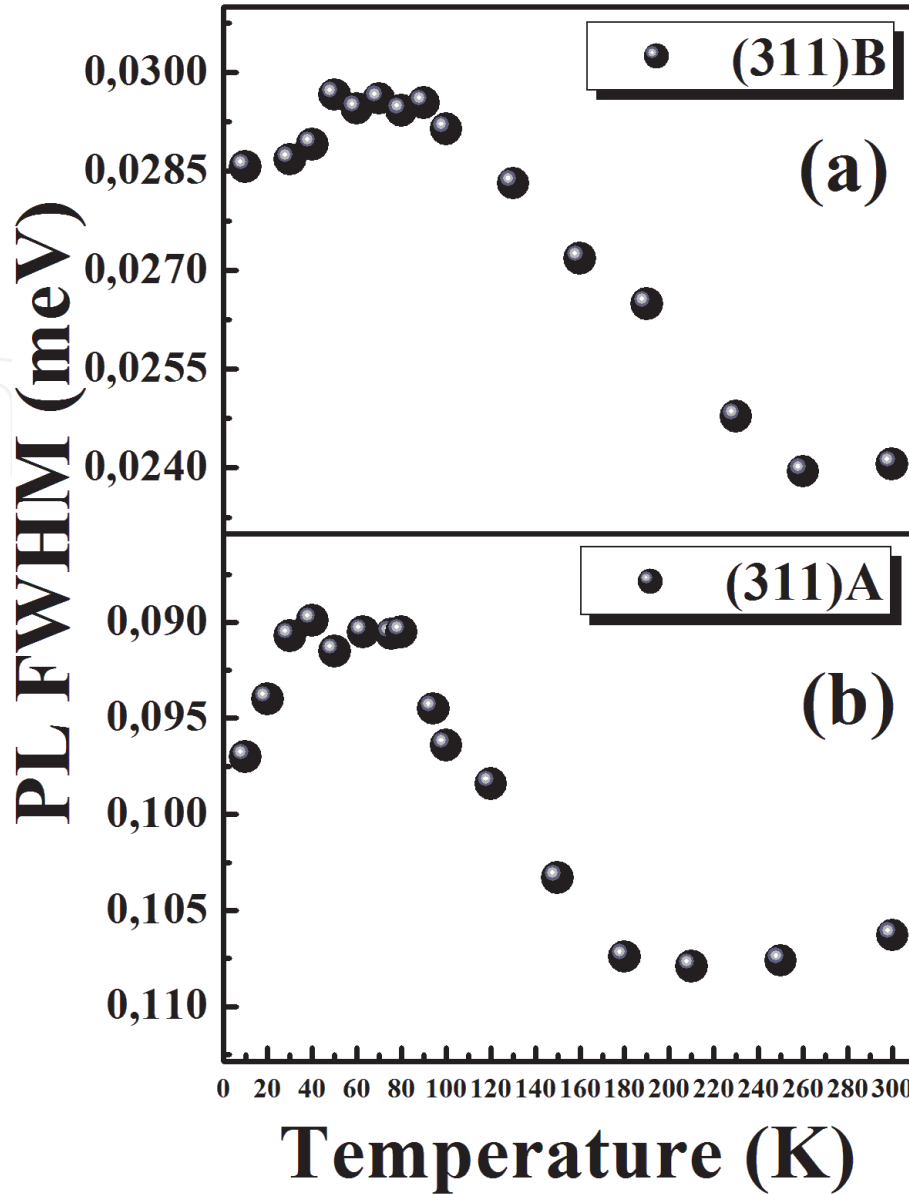


Figure 8.

(a) and (b) Evolution of the FWHM dependence of transition type II emission in $\text{In}_{0.513}\text{Al}_{0.487}\text{As}$ grown on InP (311) B and on InP (311) A substrates, respectively.

considering the polarity of the surface [In-rich (A) or P-rich (B)] from which the distinction of the PZ field within both structures [1, 18]. In the growth of the high index plane (311), the PZ field and an internal field are along the same direction (polarity A) [18, 19]. In fact, carriers can be easily delocalized due to the strong phonon coupling carrier, which is an important channel for carrier transfer in-plane hopping effect [24]. In comparison, field direction is opposite in polarity B (see **Figure 3**) [25, 34]. Due to the PZ field effect, the impact of localization is affected by interface undulation in this phase. Furthermore, the amount of alloy fluctuations in the composition of the material and the exchange of P-As.

3.2 Photoreflectance study

PR measurements were performed at room temperature to explore the evolution of the optical properties of the InAlAs/InP heterostructures during the development phase. The received PR spectra are described in **Figure 9**, with a distinct V/III ratio and substrate polarity. The PR spectra show a transition varying between 1.18 and 1.21 eV for samples S1, S1', S2 and S2'. We suggest that this peak is related to the

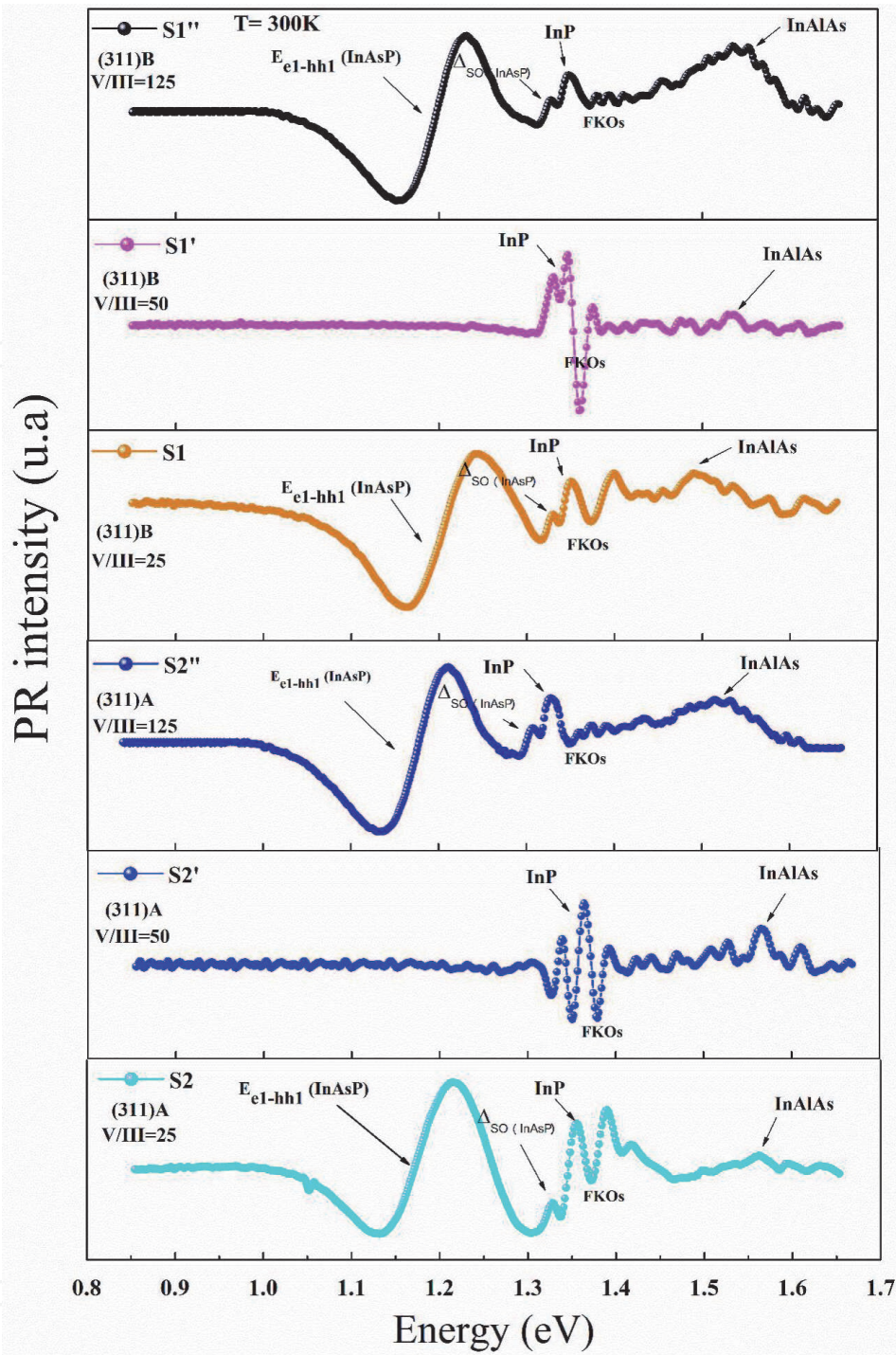


Figure 9. Room-temperature PR spectra for InAlAs layers grown on (311) B (samples S1, S1' and S1'') and (311) A (samples S2, S2' and S2'') InP substrates with different V/III ratio molar.

emission (1e-1h) between electron sub band and light-hole sub-band of quantum well (QW) InAsP [5]. While the spin split-off band of the InAsP layers lies at about 1.32 eV. On the other side, for the samples (S1', S2'), these two peaks totally disappear with a V/III ratio of 50 [5]. This result can be related during the growth to the uniformity of the inverse interface between InAlAs and InP. Furthermore, we noted that PR spectra of all samples show an additional above-band-gap (E_0 InP) characteristics that are Franz-Keldysh oscillations (FKO), reflecting the presence of a built-in electric field in the InP substrates [5, 35]. Finally, it is possible to attribute the peak exposed between 1.5 and 1.56 eV to the InAlAs band gap transition [19]. The origin of this very wide range is associated with the existence of the clustering phenomenon in the layer $\text{In}_x\text{Al}_{1-x}\text{As}$ caused by the fluctuation of the indium composition [19].

In order to assess the electrical field quality of each InP substrate, the FKO period is evaluated using an asymptotic expression for the PR spectrum provided in [36, 37]. In this strategy, InP FKO is indicated by:

$$\frac{\Delta R}{R} \propto \frac{1}{E^2(E - E_0)} \exp \left[-2(E - E_0)^{1/2} \frac{\Gamma}{(\square\Omega)^{3/2}} \right] \cos \left[\frac{4}{3} \left(\frac{E - E_0}{\hbar\Omega} \right)^{3/2} + \phi \right] \quad (2)$$

where E_0 is the transition energy, ϕ is an arbitrary phase factor, Γ is the linewidth broadening.

According to the asymptotic Franz-Keldysh model [37], the energy of oscillation extrema is given by:

$$E_m = (\square\Omega)H_m + E_0 \quad (3)$$

where $H_m = \left[\left(\frac{3m}{2} \right) (m - 1/2) \right]^{2/3}$ and m ($m \geq 1$) denotes the m th FKO extremum. E_0 is the band-gap energy (InP) and $\square\Omega$ is the electro-optic energy expressed as takes after:

$$\square\Omega = \left(\frac{q^2 \hbar^2 F_{int}^2}{8\mu} \right)^{1/3} \quad (4)$$

Noting that q is the electron charge, μ is the reduced inter-band effective mass in the electric field direction, \hbar is the reduced Planck constant, and F_{int} is the internal electric field.

Thus, by plotting E_m as a function of H_m , from linear fitting, we can decide $\square\Omega$ and E_0 from the slope and the intersection with the ordinate at the origin, respectively. Recalling Eq. (4), F_{int} can be calculated by:

$$F_{int} = \sqrt{\frac{8\mu(\hbar\Omega)^3}{q^2 \hbar^2}} \quad (5)$$

Plotted in **Figure 10** is the intercept E_0 of the best linear adjustments of the variation of E_n as a function of H_n for all samples [5]. Then, E_0 was the intercept defined from the best linear adjustment of E_n (H_n) plot, whereas $\square\Omega$ is simply the slope of the linear fit. **Table 2** shows the acquired values of transitions E_0 (InP) discovered by this fitting procedure and the FKOs analysis method.

From Eq. (3), a plot of E_m vs H_m is a straight line, and the electric field strength F_{int} can be acquired from the plot slope. **Figure 10** shows the graphs of E_m vs H_m for all samples with their corresponding linear fits. The residual strain in (311) A/B-oriented samples will generate a PZ field contributing to the F_{int} electrical field built-in InP. We assumed F_{int} was the sum of the PZ and built-in electrical fields. So, with regard to built-in electrical fields, the PZ field component predominates. The integrated electric field F_{int} is therefore equal to the PZ areas [5].

The values acquired from the above-explained FKO evaluation of the built-in electrical field strength are provided in **Table 2**. We discovered that when the orientation of the substrate changes, the F_{int} is modified, which suggests PZ impacts in the samples. The estimated PZ field is of about 36.27, 20.53, 8.11, 25.44, and 32.86 KV/cm for samples S1, S1', S1'', S2, and S2', respectively. Our findings will show that the PZ field is very susceptible to growth conditions in the InAlAs/InP samples [5].

Figure 11 shows the dependency of the PZ field in the studied samples on the polarity of the InP substrate and the V/III ratio. It is obviously noted that the PZ

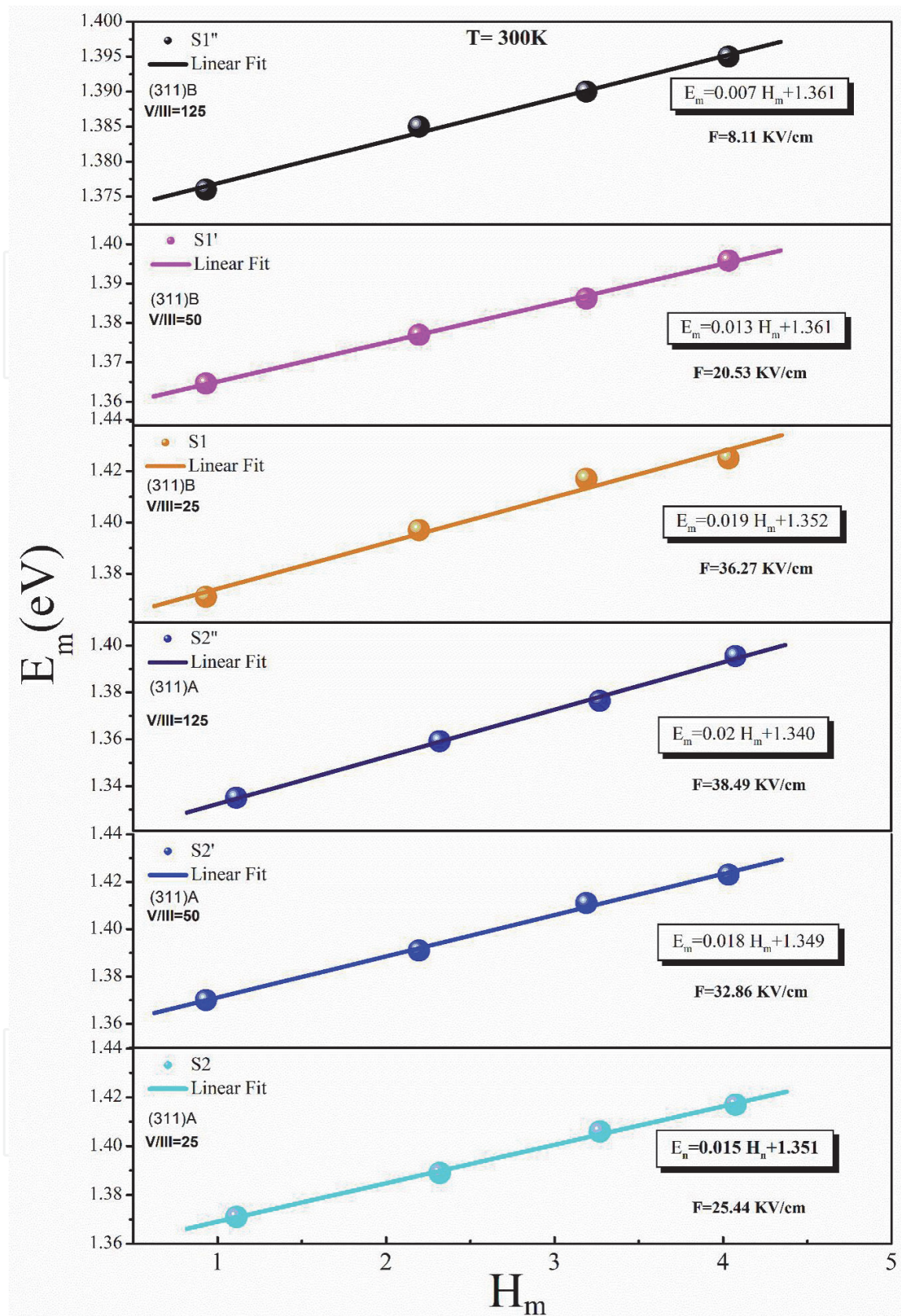


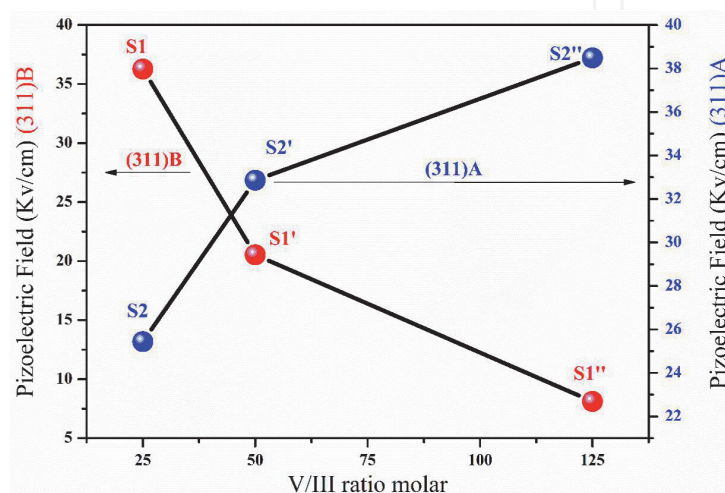
Figure 10. FKO analysis for samples S1, S1', S1'', S2, S2', and S2''. Symbols are the energies of the FKO Extrema E_n as a function of $H_n = \left[\left(\frac{3H}{2}\right)(n - 1/2)\right]^{2/3}$. Solid lines are the linear fit using Eq. (2).

field drops with increasing the V/III ratio molar for the orientation (311) B [5]. The S1 sample indicates a comparatively powerful PZ field. As the V/III ratio increases, the PZ field decreases rapidly to reach 20.53 KV/cm for sample S1' (V/III = 50) and 8.11 KV/cm for sample S1'' (V/III = 125). In comparison, for (311) A-surface, we

Samples	Substrate orientation	E_0 (InP) (eV)	F_{int} (KV/cm)
S1	(311) B	1.352	36.27
S1'	(311) B	1.396	20.53
S1''	(311) B	1.361	8.11
S2	(311) A	1.351	25.44
S2'	(311) A	1.349	32.86
S2''	(311) A	1.340	38.49

Table 2.

Summary of energy gap (E_g) and the piezoelectric field (F_{pz}) values obtained from photoreflectance PR with different V/III ratio molar.

**Figure 11.**

Piezoelectric field dependence on the V/III ratio molar for (311) A (closed circles blue) and (311) B (closed circles red) substrate orientation.

noted an increase in the PZ field as the V/III ratio increases. It increases from 25.44 to 32.86 KV/cm when the V/III ratio increases almost twice [5].

From the surface kinetics aspect, it is possible to understand this difference in the variation of the PZ field with the V/III ratio for (311) A and (311) B orientation. The sign of the PZ charge is based on the atomic composition of the interfaces [38–40]. Therefore, it is necessary to distinguish between the substrates In planes, alluded to as (N11) A plane, and the planes P, alluded to as (N11) B-planes. The single-bond sites on a (311) surface are P sites and the double-bond sites are In locations. On the contrary, the surface (311) B has an inverse bonding arrangement as shown in **Figure 5** [5, 19]. Therefore, for (311) A-face, less As atoms appear to close the cultivated surface at a small V/III ratio. Because of the stronger bond strength of Al-As than In-As, additional As atoms bond to Al statistically, bringing about more AlAs. Therefore, when V/III decreases, the coefficient of incorporation decreases [5]. By contrast, if the V/III ratio increases, though the tendency of As to combining with Al is still high, because of this oversupply, In atoms have more opportunity to bond with As atoms. In this way, the In incorporation coefficient increases with V/III ratio [5], which creates an increase in the PZ field with V/III ratio for the (311) A-oriented samples (S2 and S2'). Furthermore, we noted the opposite phenomenon of what is occurring for (311) B-face. The PZ field in our samples cultivated on (311) A substrate has the opposite direction than for (311) B [5].

We plotted the type II transition energy with the field for both the A and B polarity substrates in order to estimate the role of the PZ field (see **Figure 11**). The

shift in energy owing to the PZ field has a distinct impact on the termination of the substrates A and B [1, 5]. This is because the PZ field may increase or decrease the space separation of the electron/hole that already exists because of the strain [41]. Consequently, the band structures of the InP/InAlAs/InP samples are plotted schematically of the inset of **Figure 2**. Based on the orientation of the substrate, the band diagrams are shifted to the left side while for (311) A and shifted to the right side for (311) B due to the presence of the PZ field [1, 5]. Finally, based on the discourse in previous parts, it can be concluded that the red shift in the type II recombination for the (311) A and the blue shift for the (311) B orientation with an increasing V/III ratio is related to the meaning of the PZ field. Another possible reason for the shift of type-II transition is the difference of exchange As/P at the InAlAs/InP interface resulting from a different polarity of InP [1, 5].

4. Conclusion


In summary, InAlAs/InP type-II heterostructures with a varying V/III ratio grown successfully on (311) A or B Fe-doped InP substrates by MOCVD were investigated and the optical properties of the grown structures were examined. The different optical properties of the samples grown on (311) A or B substrates are caused from the difference of their plane-bonding configurations. In particular, the optical properties of InAlAs-InP interface display a significant reliance on AsH₃ overpressure and substrate polarity. PL and PR measurements indicated that substrate orientation and V/III ratio molar have an important impact on the quality of inverted interface. The measurements of excitation power density PL confirm the intrinsic transition of type II. A red shift of the type-II transition was noted at low temperature with an increased V/III ratio of the polarity A samples and a blue shift for polarity B samples. These findings could be clarified by the opposite field of PZ at the heterostructures of InAlAs/InP resulting from distinct polarity of the InP substrate. We acquired the InP field built-in PZ in the heterostructures from an assessment by the FKO. We have made an explanation of the transition shift from these values. Additionally, the temperature variety shows an anomalous S-shaped dependence that is typical of carrier localization in the material. The optical properties are significantly influenced by the PZ field in our samples. Therefore, the impact of the PZ field on the design and manufacture of greater quality instruments should be taken into consideration.

Author details

Badreddine Smiri*, Faouzi Saidi and Hassen Maaref
Laboratoire des Micro-optoélectroniques et Nanostructures, Faculté des Sciences
Monastir, Université de Monastir, Monastir, Tunisia

*Address all correspondence to: badreddinesmiri@gmail.com

IntechOpen

© 2020 The Author(s). Licensee IntechOpen. This chapter is distributed under the terms of the Creative Commons Attribution License (<http://creativecommons.org/licenses/by/3.0>), which permits unrestricted use, distribution, and reproduction in any medium, provided the original work is properly cited. 

References

- [1] Smiri B, Fraj I, Saidi F, Mghaïth R, Maaref H. Effect of piezoelectric field on type II transition in InAlAs/InP (311) alloys with different substrate polarity. *Journal of Alloys and Compounds*. 2018; **736**:29-34
- [2] Cornet C, Schliwa A, Even J, Doré F, Celebi C, Létoublon A, et al. Electronic and optical properties of InAs/InP quantum dots on InP(100) and InP(311) B substrates: Theory and experiment. *Physical Review B*. 2006;**74**:035312
- [3] Kawamura Y, Kamada A, Yoshimatsu K, Kobayashi H, Iwamura H, Inoue N. Photoluminescence study of interfaces between heavily doped AlInAs:Si layers and InP (Fe) substrates. *Institute of Physics Conference Series*. 1997;**155**:129
- [4] Yerino CD, Liang B, Huffaker DL, Simmonds J, Lee ML. Molecular beam epitaxy of lattice-matched InAlAs and InGaAs layers on InP (111) A, (111) B, and (110). *Journal of Vacuum Science and Technology B*. 2017;**35**:010801
- [5] Smiri B, Fraj I, Bouzidi M, Saidi F, Rebey A, Maaref H. Effect of V/III ratio on the optical properties of (311) A and (311) B oriented InAlAs/InP heterostructures. *Results in Physics*. 2019;**12**:2175-2182
- [6] Hellara J, Borgi K, Maaref H, Souliere V, Monteil Y. Optical properties of InP/InAlAs/InP grown by MOCVD on (100) substrates: Influence of V/III molar ratio. *Journal of Materials Science and Engineering C*. 2002;**21**:231-236
- [7] Wang CA, Goyal A, Huang R, Donnelly J, Calawa D, Turner G, et al. Strain-compensated GaInAs/AlInAs/InP quantum cascade laser materials. *Journal of Crystal Growth*. 2010;**312**:1157-1164
- [8] Bohrer J, Krost A, Heitz R, Heinrichsdorff F, Eckey L, Bimberg D, et al. Interface inequivalence of the InP/InAlAs/InP staggered double heterostructure grown by metalorganic chemical vapor deposition. *Journal of Applied Physics Letters*. 1996;**68**:1072
- [9] Demir I, Elagoz S. V/III ratio effects on high quality InAlAs for quantum cascade laser structures. *Journal of Superlattices and Microstructures*. 2017; **104**:140-148
- [10] Czuba K, Jurencyk J, Kaniewski J. A study of InGaAs/InAlAs/InP avalanche photodiode. *Solid-State Electronics*. 2015;**104**:109-115
- [11] Chevallier CB, Baltagi Y, Guillot G, Hong K, Pavlidis D. Application of Photoreflectance spectroscopy to the study of interface roughness in InGaAs/InAlAs/InGaAs/InAlAs heterointerfaces. *Journal of Applied Physics*. 1998;**84**:5291
- [12] Ajayan J, Nirmal D. A review of InP/InAlAs/InGaAs based transistors for high frequency applications. *Journal of Superlattices and Microstructures*. 2015; **86**:1-19
- [13] Reynolds DC, Bajaj KK, Litton CW, Yu PW, Maselink WT, Rischer R, et al. Sharp-line photoluminescence spectra from GaAs-GaAlAs multiple-quantum-well structures. *Journal of Physics. Review B*. 1984;**29**:7038-7041
- [14] Kuriharaa K, Takashimab M, Sakatab K, Uedab R, Takaharab M, Ikedab H, et al. Phase separation in InAlAs grown by MOVPE with a low growth temperature. *Journal of Crystal Growth*. 2004;**271**:341-347
- [15] Vignaud D, Wallart X, Mollot F, Sermage B. Photoluminescence study of the interface in type II InAlAs-InP heterostructures. *Journal of Applied Physical*. 1998;**84**:2138-2145
- [16] Fraj I, Hidouri T, Saidi F, Maaref H. Carrier localization localization in

In_{0.21}Ga_{0.79}As/GaAs multiple quantum wells: A modified Passler model for the S-shaped temperature dependence of photoluminescence energy. *Superlattices and Microstructures*. 2017;**102**:351-358

[17] Teodoro MD, Dias IFL, Laureto E, Duarte JL, González-Borrero PP, Lourenço SA, et al. Substrate orientation effect on potential fluctuations in multiquantum wells of GaAs/AlGaAs. *Journal of Applied Physics*. 2008;**103**: 093508

[18] Smiri B, Hidouri T, Hassen Maaref SF. Carriers' localization and thermal redistribution in InAlAs/InP grown by MOCVD on (311)A- and (311)B-InP substrates. *Applied Physics A: Materials Science & Processing*. 2019;**125**:134

[19] Smiri B, Saidi F, Mlayah A, Maaref H. Effect of substrate polarity on the optical and vibrational properties of (311)A and (311) B oriented InAlAs/InP heterostructures. *Physica E: Low-dimensional Systems and Nanostructures*. 2019;**112**:121-127

[20] Abraham P, Monteil Y, Sacilotti M. Optical studies of InP/InAlAs/InP interface recombinations. *Journal of Applied Surface Science*. 1993;**65-66**: 777-783

[21] Poças LC, Duarte JL, Dias IFL, Laureto E, Lourenço SA, Tuginho Filho DO, et al. Photoluminescence study of interfaces between heavily doped Al_{0.48}In_{0.52}As: Si layers and InP (Fe) substrates. *Journal of Applied Physics*. 2002;**91**:8999

[22] Ezzedini M, Bouzidi M, Qaid MM, Chine Z, Rebey A, Sfaxi L. Comprehensive study of the structural, optical and electrical properties of InAlAs: Mg films lattice matched to InP grown by MOVPE. *Journal of Materials Science: Materials in Electronics*. 2017; **18**:18221-18227

[23] Sayari A, Yahyaoui N, Meftah A, Sfaxi A, Oueslati M. Residual strain and alloying effects on the vibrational properties of step-graded In_xAl_{1-x}As layers grown on GaAs. *Journal of Luminescence*. 2009;**129**:105-109

[24] Li Y, Niewcza M. Strain relaxation in (100) and (311) GaP/GaAs thin films. *Journal of Applied Physics*. 2007; **101**:064910

[25] Tromson-Carli A, Patriarche G, Druilhe R, Lusson A, Marfaing Y, Triboulet R, et al. Effect of the {h11} orientations and polarities of GaAs substrates CdTe buffer layer structural properties. *Journal of Materials Science and Engineering B*. 1993;**16**:145-150

[26] Peter M, Herres N, Fuchs F, Winkler K, Bachem K-H, Wagner J. Band gaps and band offsets in strained GaAs(1-y)Sb(y) on InP grown by metalorganic chemical vapor deposition. *Applied Physics Letters*. 1999;**74**: 410-412

[27] Hu J, Xu G, Stotz J, Watkins S, Curzon A, Thewalt M, et al. Type II photoluminescence and conduction band offsets of GaAsSb/InGaAs and GaAsSb/InP heterostructures grown by metalorganic vapor phase epitaxy. *Applied Physics Letters*. 1998;**73**:2799

[28] Shuhui Z, Lu W, Zhenwu S, Yanxiang C, Haitao T, Huaiju G, et al. Lattice parameter accommodation between GaAs(111) nanowires and Si (111) substrate after growth via Au-assisted molecular beam epitaxy. *Nanoscale Research Letters*. 2012; **7**(1):109

[29] Ferguson I, Cheng T, Sotomayor Torres C, Murray R. Photoluminescence of molecular beam epitaxial grown Al_{0.48}In_{0.52}As. *Journal of Vacuum Science and Technology B*. 1994;**12**:1319

[30] Merkel K, Bright V, Cerny C, Shcuermeyer F, Solomon J, Kaspi R.

Beryllium ion implantation in GaAsSb epilayers on InP. *Journal of Applied Physics*. 1995;**79**:699

[31] Chouaib H, Bru-Chevallier C, Guillot G, Lahreche H, Bove P. Photoreflectance study of GaAsSb/InP heterostructures. *Journal of Applied Physics*. 2005;**98**:123524

[32] Saidi F, Hamila R, Maaref H, Rodriguez P, Auvray L, Monteil Y. Structural and optical study of $BxInyGa_{1-x-y}As/GaAs$ and $InyGa_{1-y}As/GaAs$ QW's grown by MOCVD. *Journal of Alloys and Compounds*. 2010;**491**:45-48

[33] Hamila R, Saidi F, Maaref H, Rodriguez P, Auvray L. Photoluminescence properties and high resolution X-ray diffraction investigation of $BInGaAs/GaAs$ grown by the metalorganic vapour phase epitaxy method. *Journal of Applied Physics*. 2012;**112**:063109

[34] Hou HQ, Tu CW. Field screening in (111)B InAsP/InP strained quantum wells. *Journal of Electronic Materials*. 1996;**25**:1019-1022

[35] Nukeaw J, Matsubara N, Fujiwara Y, Takeda Y. Characterization of InP δ -doped with Er by FFT photoreflectance. *Applied Surface Science*. 1997;**117/118**:776-780

[36] Bouzidi M, Benzarti Z, Halidou I, Soltani S, Chine Z, Jani BEL. Photoreflectance investigation of band gap renormalization and the Burstein-Moss effect in Si doped GaN grown by MOVPE. *Materials Science in Semiconductor Processing*. 2016;**42**:273-276

[37] Bilel C, Fitouri H, Zaied I, Bchetnia A, Rebey A, El Jani B. Photoreflectance characterization of vanadium-doped GaAs layers grown by metalorganic vapor phase epitaxy. *Journal of Materials Science in Semiconductor Processing*. 2015;**31**:100-105

[38] Sanguinetti S, Gurioli M, Grilli E, Guzzi M, Henini M. Piezoelectric-induced quantum-confined Stark effect in self-assembled InAs quantum dots grown on (N11) GaAs substrates. *Journal of Applied Physics Letters*. 2000;**77**:1982

[39] Anufriev R, Chauvin N, Khmissi H, Naji K, Patriarche G, Gendry M, et al. Piezoelectric effect in InAs/InP quantum rod nanowires grown on silicon substrate. *Journal of Applied Physics Letters*. 2014;**104**:183101

[40] Kwak JS, Lee KY, Han JY, Cho J, Chae S, Nam OH, et al. Crystal-polarity dependence of Ti/Al contacts to freestanding n-GaN-GaN substrate. *Journal of Applied Physics Letters*. 2001;**79**:3254

[41] Sacilotti M, Chaumont D, Brainer Mota C, Vasconcelos T, Nunes FD, Pompelli MF, et al. Interface recombination & emission applied to explain photosynthetic mechanisms for (e^- , h^+) charges' separation. *World Journal of Nano Science and Engineering*. 2012;**2**:58-87